Characterization of 3 PET tracers for Quantification of Mitochondrial and Synaptic function in Healthy Human Brain: ^{18}F-BCPP-EF, ^{11}C-SA-4503, ^{11}C-UCB-J

Ayla Mansur[1,2,3], Eugenii A. Rabiner[1,3,4] , Robert A. Comley[3,5], Yvonne Lewis[1.3],Lefkos T. Middleton[3,6], Mickael Huiban[1,3] , Jan Passchier [1,2,3.], Hideo Tsukada[3,7] , Roger N. Gunn[1,2,3]and MIND MAPS Consortium[3]

[1]Invicro LLC

[2] Division of Brain Sciences, Imperial College London,UK

[3]MIND MAPS Consortium: Laurent Martarello, Biogen; Robert A. Comley, AbbVie; Laigao Chen, Pfizer, Adam Schwarz, Takeda; Karl Schmidt, Celgene; Paul Matthews, Imperial College London; Marios Politis, King's College London; Jonathan Rohrer, University College London; David Brooks, Newcastle University; James Rowe, University of Cambridge.

[4]King's College London, UK

[5]Abbvie

[6]Neuroepidemiology and Ageing Research Unit, Imperial College London, UK

[7]Hamamatsu Photonics

*Correspondence should be addressed to Ayla Mansur, PhD candidate, Imperial College London, Division of Brain Sciences, Hammersmith Hospital London, W12 0NN, UK. +44208 008 6045 Email:ayla.mansur@invicro.co.uk

Short running title: Mitochondria and Synaptic PET Biomarkers

Financial Support: The project was funded by the MIND MAPS consortium,

Word Count: 5057

ABSTRACT

Mitochondrial complex 1 (MC1) is involved in maintaining brain bioenergetics, the sigma 1 receptor (σ1R) responds to neuronal stress and synaptic vesicle protein 2A (SV2A) reflects synaptic integrity. Expression of each of these proteins is altered in neurodegenerative diseases. Here we characterise the kinetic behaviour of three positron emission tomography (PET) radioligands ^{18}F-BCPP-EF, ^{11}C-SA-4503 and ^{11}C-UCB-J, for the measurement of MC1, σ1R and SV2A, respectively, and determine appropriate analysis workflows for their application in future studies of the *in vivo* molecular pathology of these diseases. **Methods:** Twelve human subjects underwent dynamic PET scans including associated arterial blood sampling with each of the radioligands. A range of kinetic models were investigated in order to identify an optimal kinetic analysis method for each radioligand and enable the identification of a suitable acquisition duration. **Results:** All three radioligands readily entered the brain and yielded heterogeneous uptake consistent with the known distribution of the protein targets. The optimal models determined for the regional estimates of volume of distribution (V_T) were multilinear analysis 1 (MA1) and the 2-tissue compartment (2TC) model for ^{18}F-BCPP-EF, MA1 for ^{11}C-SA-4503, and both MA1 and the 1-tissue compartment (1TC) model for ^{11}C-UCB-J. Acquisition times of 70, 80 and 60 minutes for ^{18}F-BCPP-EF, ^{11}C-SA-4503, ^{11}C-UCB-J, respectively, provided good estimates of regional V_T values. An effect of age was observed on ^{18}F-BCPP-EF and ^{11}C-UCB-J signal in the caudate. **Conclusion:** These ligands can be assessed for their potential to stratify patients or monitor the progression of molecular neuropathology in neurodegenerative diseases.

Keywords Kinetic modelling, neurodegeneration, synapses, mitochondria, endoplasmic reticulum

INTRODUCTION

The complex and heterogeneous pathophysiology of neurodegenerative diseases represents a major challenge for the discovery and development of disease modifying therapeutics. A growing body of literature implicates cellular stress-related mitochondrial and endoplasmic reticulum (ER) dysfunction and related synaptic abnormalities as a common denominator across neurodegenerative diseases, making the mitochondrial/ER/synapse axis an attractive system to target in the search for biomarkers that can be used to monitor disease progression (*1–3*). Mitochondrial ATP production is critical for the bulk of neuronal processes, including neurotransmitter synthesis and synaptic plasticity. The mitochondrial complex 1 (MC1) is a critical component of ATP production, as it is where the first step of oxidative phosphorylation takes place (*4*). MC1 is responsible for cellular house-keeping mechanisms such as maintaining cellular calcium (Ca^{+2}) homeostasis, producing reactive oxygen and nitrogen species and regulating apoptosis (*4*). Altered MC1 function has been associated with cell toxicity, accelerated aging and the pathogenesis of multiple neurodegenerative diseases (*1*). *In vivo* quantification of MC1 in the brain has been made possible with the development of PET radioligand ^{18}F-BCPP-EF (*5*). Characterisation of ^{18}F-BCPP-EF kinetics in the non-human primate (NHP) brain has suggested its suitability for human evaluation, but no human data has been published to date (*6*,*7*).

A second regulator of cellular energy is the sigma 1 receptor (σ1R) which is a chaperone protein that stabilises the inositol phosphate 3 receptor (IP3R)/voltage dependent anion channel (VDAC) in the mitochondria-associated ER membrane (MAM) (*8*). This IP3R-VDAC channel is the principal pathway for Ca^{+2} influx from the ER stores to the mitochondrion, with ATP production rate depending significantly on Ca^{+2} concentration (*9*). σ1R is involved in protein sorting and folding, synaptic plasticity and neuro-protection, with human post-mortem evidence of altered expression in Alzheimer's disease (*10–12*). Early PET imaging studies have used the radioligand ^{11}C-SA-4503 to evaluate σ1R status in healthy, Parkinson's and Alzheimer's disease cohorts, though an evaluation of the optimal imaging methodology for ^{11}C-SA-4503 has yet to be established (*13–15*).

The synaptic vesicle protein A (SV2A) is a membrane glycoprotein expressed ubiquitously on synaptic vesicles in presynaptic terminals and regulates Ca^{+2} mediated neurotransmitter release (*16*). SV2A has been shown to have a stable synaptic stoichiometry with good correlation to recognised synaptic density markers such as synaptophysin, and thus offers great promise as a marker of synaptic

terminal density in the human brain (*17*). Synaptic loss is central to all neurodegenerative diseases pathology, with changes to presynaptic structure and function evident in presymptomatic stages of disease, raising interest in the use of SV2A markers (*18–20*). Quantification of SV2A has been made possible with the discovery of novel radioligand ^{11}C-UCB-J, with recent findings indicating a reduction in ^{11}C-UCB-J specific binding in healthy aging, as well as patients with mild cognitive impairment and AD has demonstrated excellent imaging characteristics (*21–23*).

The availability of PET radioligands ^{18}F-BCPP-EF, ^{11}C-SA4503 and ^{11}C-UCB-J enables the quantification of MC1, σ1R and SV2A, respectively, and allows us to test the hypothesis that a combination of these markers could provide a useful index of the function of the mitochondrial/ER/synapse axis depicted in Figure 1. The data utilised in this manuscript was collected from twelve healthy volunteers as part of the MINDMAPS consortium (www.invicro.com/MINDMAPS). The methods identified here will be used for the future quantification of healthy volunteer and patient cohorts in the MINDMAPS programme. The primary aim is to establish an appropriate set of image analysis workflows including optimal tracer kinetic quantification approaches and outcome measures for ^{18}F-BCPP-EF, ^{11}C-SA-4503 and ^{11}C-UCB-J in humans. A secondary aim is to explore whether MC1, σ1R and SV2A expression is altered in healthy aging.

MATERIALS AND METHODS

Study Design

All procedures followed were in accordance with the ethical standards of East of England - Cambridge South Research Ethics Committee and with the Helsinki Declaration of 1975, as revised in 2008. Data from 12 participants (7M/5F, 61±20 years, range 33-75) from ongoing studies evaluating MC1, SV2A and σ1R density in healthy volunteers, was included in this manuscript. Subjects were screened and scanned at Invicro London's Hammersmith Hospital site. Each subject's data acquisition included a structural MRI of the brain during screening and one PET scan with each of the following radioligands: ^{18}F-BCPP-EF, ^{11}C-SA-4503 and ^{11}C-UCB-J. Written informed consent was obtained from all subjects.

Radiotracer Synthesis

^{18}F-BCPP-EF, ^{11}C-SA-4503 and ^{11}C-UCB-J were synthesised as previously described (*5*,*24*,*25*). Tracer injected dose information for each radioligand is summarised in Supplemental Table 1.

PET Acquisition

All PET scans were acquired on either a Siemens Hi-Rez Biograph 6 or Biograph 6 TruePoint PET/CT scanner (Siemens Healthcare, Erlangen, Germany) with subjects receiving all 3 PET scans on the same scanner. A low-dose Computed Tomography (CT) scan (30 mAs, 130 KeV, 0.55 pitch) was performed immediately before each PET scan in order to estimate attenuation. An intravenous cannula was inserted into a cubital or forearm vein for radioligand administration, and a second cannula was inserted into the radial artery to enable arterial blood collection. The radioligands were administered as a bolus (over 20 seconds) in a volume of 20 mL at the start of the PET scan. Dynamic emission data were acquired over 90 minutes following radiotracer administration and were reconstructed into 26 frames (frame durations: 8x15 s, 3 x 60 s, 5 x 120 s, 5 x 300 s, 5 x 600 s) using Discrete Inverse Fourier Transform reconstruction. Corrections were applied for attenuation, randoms and scatter.

Arterial Blood Acquisition

Arterial blood was taken for the estimation of total radioactivity concentration in whole blood and plasma, and the fraction of the total radioactivity constituted by the parent radioligand (*ppf*). For each ligand, the plasma free fraction (f_p) was measured by ultrafiltration in triplicate using an arterial blood sample taken prior to tracer injection. Additional details are provided in the supplemental materials.

MR Acquisition

Each subject had a T1-weighted MRI scan for coregistration with PET images. Scans were acquired on a Siemens 3T Trio clinical MRI scanner (Siemens Healthineers, Erlangen, Germany) with a 32-channel phased-array head coil using a 3D MPRAGE sequence (TE = 2.98 ms, TR = 2300 ms, cflip angle of 9^o, voxel size = 1.0 mm x1.0 mm x1.0 mm).

Image Analysis and Processing

All image data were analysed using Invicro London's in-house PET data quantification tool, MIAKAT^{TM} (version 4.3.7, http://www.miakat.org), that implements MATLAB (version R2016a; Mathworks Inc., Natick, MA, USA), FSL (version 5.0.4; FMRIB, Oxford, UK) functions for brain

extraction and SPM12 (Wellcome Trust Centre for Neuroimaging, http://www.fil.ion.ucl.ac.uk/spm) for image segmentation and registration (*26*).

Each subject's MRI underwent brain extraction, grey matter (GM) segmentation and rigid body coregistration to a standard reference space (*27*). The template brain image and associated CIC atlas was then nonlinearly warped to the individual subject's MRI image where the following regions of interest (ROI) were defined: brainstem, substantia nigra, thalamus, ventral striatum, caudate, putamen, hippocampus, insular cortex, temporal lobe, parietal lobe, frontal cortex and the cerebellum (*28*). A centrum semiovale ROI was also generated from the automated anatomic labelling (AAL) template as defined previously for investigation as a reference region for ^{11}C-UCJ-J (*21*,*29*). PET images were registered to each subject's MRI image and corrected for motion using frame-to-frame rigid-body registration. Regional time activity curves (TAC) were generated for each ROI.

Arterial Input Function Modelling

Discrete blood samples acquired during the PET scan were fitted with a linear, constant and exponential model to determine the *ppf*. Optimal models were identified for each tracer and applied to the total plasma activity curve to derive a metabolite corrected arterial input function.

Tracer Kinetic Modelling

All TACs were fitted with a one-tissue compartment (1TC) model, a two tissue compartment (2TC) model and multilinear analysis 1 (MA1) to estimate the volume of distribution (V_T) (*30*). MA1 was applied to TAC data with integration intervals computed over 30-90 minutes for all tracers based on an initial assessment of an appropriate temporal window. Blood volume fraction was fixed to 5% during parameter estimation. V_T/f_p was also assessed as an outcome measure to explore its utility in studies where there are differences in f_p values.

Given the low white matter uptake we observed for ^{18}F-BCPP-EF, ^{11}C-SA-4503 and ^{11}C-UCB-J, we assessed the centrum semiovale as a pseudo-reference region for each ligand, and used it to calculate the distribution volume ratio (DVR).

Model Comparison and Selection

The performance of 1TC and 2TC models was assessed by Akaike Information Criteria (AIC) and parameter identifiability based on the percentage standard error (SE%) derived from the covariance matrix (*31*). Linear regression correlation coefficients (r^2) were used to compare performance between the graphical method MA1 and the compartmental models. V_Ts that were poorly estimated (SE%>10) were excluded from model comparisons.

Time Stability Analysis

The stability of each radiotracer over time was evaluated by exploring the performance of the tracer kinetic analysis methods for varying scan lengths. The estimated V_T values were expressed as percentages of the V_T estimated from the full 90 min scan (V_T^{90min}). These analyses were aggregated together over all subjects enabling assessment of time stability of the radiotracers in the population.

Assessment of Age Effects on Outcome Measures

A preliminary assessment of the effects of healthy aging on MC1, σ1R and SV2A density was conducted using correlation analysis with age as the predictor variable and the PET outcome measures and ROI volume as parameters of interest. ROI volume was normalised to whole brain volumes,

$$\%Vol_{roi} = 100 \times \frac{Vol_{roi}}{Vol_{brain}} \qquad \text{Equation 1}$$

where Vol_{roi} is the GM volume in a given ROI and Vol_{brain} is the whole brain volume. Percent rates of change per year in V_T, V_T/f_p, DVR and $\%Vol_{roi}$ were then calculated as,

$$\%\,\Delta/\text{year} = 100 \times \left(\frac{\Delta\text{Parameter}}{\Delta\text{Age}}\right)/\text{Parameter}_{\text{mean}} \qquad \text{Equation 2}$$

RESULTS

All twelve participants completed three 90 minute dynamic PET scans including arterial blood sampling and an MRI. A summary of demographic information and individual scan parameters for each radioligand are included in Supplemental Table 1.

Arterial Input Function Modelling

Ppf data for ^{18}F-BCPP-EF was best described by a sigmoid model with 20(8)% intact parent radiotracer at 90 minutes. ^{11}C-SA-4503 metabolite data were best described with an exponential function where *ppf* was estimated at 91(5)% at 90 minutes post-injection. ^{11}C-UCB-J metabolite data were described by a sigmoid model with approximately 25(5)% at 90 minutes. Individual *ppf* and input function profiles are shown in the Supplemental Figure 1.

Tracer Kinetic Modelling

All three tracers entered the brain readily, and demonstrated a heterogeneous distribution (Fig. 2). ^{18}F-BCPP-EF uptake was fast and peak uptake values (SUV) were reached at ~5-12 minutes post injection. ^{11}C-SA-4503 uptake was slow and reached peak uptake at ~30-60 minutes post-injection. ^{11}C-UCB-J displayed fast kinetics producing peak SUV at ~7-21 minutes post-injection.

All kinetic models tested reached convergence in the regional ^{18}F-BCPP-EF-derived TAC data (Fig. 3). V_T was robustly estimated in all ROIs explored using both 1TC and 2TC; with AIC analysis favouring the 2TC over 1TC in all cases tested. As 2TC and MA1 derived V_T were in excellent agreement (r^2 = 0.99) (Supplemental Fig. 2A), both were chosen as suitable modelling methods for ^{18}F-BCPP-EF.

For ^{11}C-SA-4503, 2TC produced the most parsimonious fits to TACs in 155/156 of the cases tested as determined by AIC when compared to 1TC, however, V_T values were poorly estimated in 17/156 cases. MA1 produced good fits to the TAC data and V_T estimates were in close agreement with those reliably estimated using the 2TC model (r^2=0.97)(Supplemental Fig. 2B), and was therefore chosen as the appropriate kinetic model for ^{11}C-SA-4503.

All 3 models produced excellent fits to ^{11}C-UCB-J TAC data. AIC preferred 2TC over 1TC in 146/156 cases, however 3/156 V_T estimates were unstable with 2TC. MA1 produced good fits which were well-correlated with 1TC fits in all regions analysed (r^2=0.99) (Supplemental Fig. 2C).

V_T estimates derived using all kinetic models are summarised for each radioligands in Table 1. The average coefficient of variance (COV) of regional V_T estimates across all regions investigated was 19(4)% for ^{18}F-BCPP-EF, 20(6)% for ^{11}C-SA-4503 and 13(5)% for ^{11}C-UCB-J (Fig. 4). There was no relationship between injected mass of radioligand and V_T estimates for any of the tracers (Supplemental Table 2).

Time Stability Analysis

For ^{18}F-BCPP-EF 70 minutes of PET data provided good stability of V_T (Fig. 5A), where the resulting V_T was 98.4(6.7)% of the final V_T. 80 minutes acquisition with ^{11}C-SA-4503 produced reliable V_T estimates that were 98.2(1.2)% of the V_T^{90min} (Fig. 5B). ^{11}C-UCB-J estimates derived from a 60 minute scan duration were 98.0(1.8)% of V_T^{90min} (Fig. 5C). Regional time stability analyses for each ligand are included in the Supplemental Figures 3-5.

Assessment of DVR and V_T/f_p as Outcome Measures

DVR results were less variable between subjects compared to the corresponding V_T estimates except for ^{11}C-SA-4503, where DVR results were more susceptible to individual differences than were the V_T estimates (Supplemental Table 3). Correction of V_T by f_p had no significant effect on inter-subject variability for any of the ligands (Supplemental Table 4).

Assessment of Age Effects on Outcome Measures

We observed a statistically significant yearly reduction in volume of 0.52% (r^2=0.50), 0.36% (r^2 =0.59) and 0.53% (r^2=0.56) in the temporal lobe, parietal lobe and frontal cortex volume, respectively (Table 2, Fig. 7A).

^{18}F-BCPP-EF V_T decreased with age most GM regions with the highest reduction of 1.68%/year (r^2=0.42) in the caudate (Fig. 6B). A similar negative trend was observed for ^{11}C-SA-4503, however none of the correlations reached significance (Fig. 6C). ^{11}C-UCB-J V_T were negatively correlated with age in all regions, with significant reductions in the thalamus, ventral striatum, caudate, insula, parietal lobe and frontal cortex (Fig. 6D; Table 2). The magnitude of the mean rates of decrease in V_T ranged from 0.48%/year (r^2=0.36) in the insula to 1.83%/year (r^2=0.68) in the caudate.

Results of our regression analysis between DVR and age were similar to those observed with V_T (Supplemental Fig. 6A; Supplemental Table 5). ^{18}F-BCPP-EF V_T/f_p was negatively correlated with

age in the thalamus, caudate, and parietal lobe while correcting ^{11}C-UCB-J V_T by f_p masked out any prior age effects on SV2A density except for in the caudate (Supplemental Fig. 6B; Supplemental Table 6). Lastly, ^{11}C-UCB-J f_p values appeared to decrease with age, though this did not reach statistical significance (Supplemental Figure 7).

DISCUSSION

The current study evaluated a variety of kinetic quantification approaches for the radioligands ^{18}F-BCPP-EF, ^{11}C-SA-4503 and ^{11}C-UCB-J in the human brain. In addition, we conducted a pilot examination of the effects of age on the density of MC1, σ1R and SV2A. ^{18}F-BCPP-EF displayed reversible kinetics with the highest uptake observed in striatal regions, consistent with NHP data (*7*). ^{18}F-BCPP-EF metabolism was rapid and the TAC data were well described using both MA1 and 2TC. Our results showed a reduction of ^{18}F-BCPP-EF with age in line with preclinical experiments (*5*). Importantly, reductions in the caudate did not appear to be driven by changes in volume (Figs. 6A and B), suggesting that striatal mitochondrial density could be particularly susceptible to aging.

The tracer characteristics of ^{11}C-SA-4503 were in agreement with initial imaging results in humans (*13*). We selected MA1 as the optimal model to describe ^{11}C-SA-4503 kinetics, as ~11% of our 2TC derived V_T estimates were poorly estimated. This was mainly due to the poor estimation of k_4 in the caudate, substantia nigra and centrum semiovale suggesting that ^{11}C-SA-4503 kinetics approach irreversibility in these regions and thus should be interpreted with caution. ^{11}C-SA-4503 signal was highest in the cerebellum, consistent with previous mouse and initial human studies (*13*,*24*). Despite preclinical reports of an age-related increase in ^{11}C-SA-4503 signal, we did not observe any such effect in our dataset.

^{11}C-UCB-J uptake was widespread and displayed fast kinetics that were well described by all three models in agreement with previous reports (*21*). Given the near perfect correlation between MA1 and 1TC derived V_T estimates, we suggest using either 1TC or MA1 for ^{11}C-UCB-J quantification. Consistent with recent reports of age effects on ^{11}C-UCB-J binding, we observed an effect of age on SV2A density in the caudate, where the reduction in signal remained significant following correction by f_p (*22*). It should be noted that with the exception of the caudate, the yearly rates of change in V_T were comparable to the rates of change in ROI volume. However, age effects on V_T remained significant for the majority of regions after controlling for $\%Vol_{roi}$ with ^{11}C-UCB-J (Supplemental Table 7).

Comparison of V_T estimates within and between groups requires the measured f_p for a particular radioligand to be unchanged between subjects or experimental conditions. In our dataset, we observed a negative effect of age on f_p for ^{11}C-UCB-J (r^2 =-0.3, p=0.10) (Supplemental Fig. 7). We therefore took V_T/f_p as the primary outcome measure. Future ^{11}C-UCB-J studies should evaluate f_p and correct for any potential differences, especially when studying patient groups.

Ideally, non-displaceable binding can be directly estimated from a reference region, which is not feasible with compounds lacking a region devoid of any binding. The use of DVR provides a partial solution to this problem by relying on a region with low specific binding, and eliminates some of the inter-subject variability in the estimation of individual input functions. Although no known reference regions exist for ^{18}F-BCPP-EF, ^{11}C-SA-4503 and ^{11}C-UCB-J, we found that ^{18}F-BCPP-EF V_T estimates in the centrum semiovale were ~50% lower than GM regions in our dataset. Similarly, ^{11}C-UCB-J V_T estimates in the centrum semiovale were ~60% lower than GM regions, supporting previous suggestions of its use as a reference region for SV2A quantification (*32*). Future blocking studies with specific MC1 and SV2A compounds should be conducted in both healthy and disease cohorts to confirm the viability of the centrum semiovale as a reference region. In the case of ^{11}C-SA-4503, V_T estimates in WM were not significantly lower than GM regions, making DVR an unsuitable outcome measure for this tracer.

Based on the results of our time stability analyses, we conclude that dynamic scanning for at least 70, 80 and 60 minutes are sufficient to reliably estimate V_T from a ^{18}F-BCPP-EF, ^{11}C-SA-4503 and ^{11}C-UCB-J scan, respectively. Our ^{11}C-UCB-J time stability results support those from a recent test-retest analysis of ^{11}C-UCB-J kinetics (*33*).

CONCLUSION

We have established a set of optimal tracer kinetic quantification models and outcome measures for ^{18}F-BCPP-EF, ^{11}C-SA-4503 and ^{11}C-UCB-J in the healthy human brain. We suggest that MA1 or 2TC can be used to quantify ^{18}F-BCPP-EF, MA1 should be used to quantify ^{11}C-SA-4503, while both MA1 and 1TC are suitable for ^{11}C-UCB-J quantification. Lastly, our analysis of the effect of age on this data set suggests that ^{18}F-BCPP-EF and ^{11}C-UCB-J signal in the caudate could serve as a marker of age-related mitochondrial dysfunction and synaptic loss.

FINANCIAL DISCLOSURE

AM, ER YL, MH, JP and RG are employees of Invicro LLC; RC is an employee of AbbVie; RG is a consultant for AbbVie, Biogen & Cerveau. HT is an employee of Hamamatsu Photonics. No potential conflicts of interest relevant to this article exist.

ACKNOWLEDGMENTS

The authors thank Elbert Perez, Ryan Janisch, and Mark Tanner for their expert assistance. The authors also thank the Yale University PET Center for provision of CS regional definition.

KEY POINTS

Question: Identification of the optimal kinetic modelling methods and outcome parameters for quantifying MC1, σ1R and SV2A density as an index of mitochondrial/ER/synaptic axis function in the healthy human brain

Pertinent Findings: In a cohort study of 12 healthy volunteers that underwent a structural MRI scan and 90 minute dynamic PET scans with ^{18}F-BCPP-EF, ^{11}C-SA-4503 and ^{11}C-UCB-J, MA1 and 2TC models best described the kinetics of ^{18}F-BCPP-EF. Reliable quantification of ^{11}C-SA-4503 was achieved using MA1, while both 1TC and MA1 were suitable for ^{11}C-UCB-J quantification.

Implications for Patient Care: The methods established here can be applied to patient cohorts assessing the same three ligands to potentially stratify patients or monitor the progression of molecular neuropathology.

REFERENCES

1. Grimm A, Eckert A. Brain aging and neurodegeneration: from a mitochondrial point of view. *J Neurochem.* 2017;143:418-431.

2. Xiang C, Wang Y, Zhang H, Han F. The role of endoplasmic reticulum stress in neurodegenerative disease. *Apoptosis*. 2017;22:1-26.

3. Briggs CA, Chakroborty S, Stutzmann GE. Emerging pathways driving early synaptic pathology in Alzheimer's disease. *Biochem Biophys Res Commun*. 2017;483:988-997.

4. Sazanov LA. A giant molecular proton pump: structure and mechanism of respiratory complex I. *Nat Rev Mol Cell Biol*. 2015;16:375-388.

5. Harada N, Nishiyama S, Kanazawa M, Tsukada H. Development of novel PET probes, [18F]BCPP-EF, [18F]BCPP-BF, and [11C]BCPP-EM for mitochondrial complex 1 imaging in the living brain. *J Label Compd Radiopharm*. 2013;56:553-561.

6. Tsukada H. The use of 18F-BCPP-EF as a PET probe for complex i activity in the brain. *Methods Enzymol*. 2014;547:417-431.

7. Tsukada H, Ohba H, Kanazawa M, Kakiuchi T, Harada N. Evaluation of 18F-BCPP-EF for mitochondrial complex 1 imaging in the brain of conscious monkeys using PET. *Eur J Nucl Med Mol Imaging*. 2014;41:755-763.

8. Hayashi T, Su TP. Sigma-1 receptor chaperones at the ER-mitochondrion interface regulate Ca(2+) signaling and cell survival. *Cell*. 2007;131:596-610.

9. Su TP, Hayashi T, Maurice T, Buch S, Ruoho AE. The sigma-1 receptor chaperone as an inter-organelle signaling modulator. *Trends Pharmacol Sci*. 2010;31:557-66.

10. Nguyen L, Lucke-Wold BP, Mookerjee S, Kaushal N, Matsumoto RR. Sigma-1

receptors and neurodegenerative diseases: Towards a hypothesis of sigma-1 receptors as amplifiers of neurodegeneration and neuroprotection. *Adv Exp Med Biol*. 2017; 964:133-152.

11. Francardo V, Bez F, Wieloch T, Nissbrandt H, Ruscher K, Cenci MA. Pharmacological stimulation of sigma-1 receptors has neurorestorative effects in experimental parkinsonism. *Brain*. 2014;137:1998-2014.

12. Jansen KLR, Faull RLM, Storey P, Leslie RA. Loss of sigma binding sites in the CA1 area of the anterior hippocampus in Alzheimer's disease correlates with CA1 pyramidal cell loss. *Brain Res*. 1993;23:299-30.

13. Sakata M, Kimura Y, Naganawa M, et al. Mapping of human cerebral sigma1 receptors using positron emission tomography and [11C]SA4503. *Neuroimage*. 2007;35:1-8.

14. Mishina M, Ishiwata K, Ishii K, et al. Function of sigma1 receptors in Parkinson's disease. *Acta Neurol Scand*. 2005;112:103-7.

15. Mishina M, Ohyama M, Ishii K, et al. Low density of sigma1 receptors in early Alzheimer's disease. *Ann Nucl Med*. 2008;22:151-156.

16. Wan QF, Zhou ZY, Thakur P, et al. SV2 Acts via presynaptic calcium to regulate neurotransmitter release. *Neuron*. 2010;66:884-895.

17. Nowack A, Yao J, Custer KL, Bajjalieh SM. SV2 regulates neurotransmitter release via multiple mechanisms. *AJP Cell Physiol*. 2010; 299:C960-7.

18. Selkoe DJ. Alzheimer's disease is a synaptic failure. *Science.* 2002; 298:789-91.

19. Reddy PH, Tripathi R, Troung Q, et al. Abnormal mitochondrial dynamics and synaptic degeneration as early events in Alzheimer's disease: Implications to mitochondria-targeted antioxidant therapeutics. *Biochim Biophys Acta Mol Basis Dis*. 2012; 1822:639-

49.

20. Milnerwood AJ, Raymond LA. Early synaptic pathophysiology in neurodegeneration: Insights from Huntington's disease. *Trends Neurosci*. 2010;33:513-2.

21. Finnema SJ, Nabulsi NB, Eid T, et al. Imaging synaptic density in the living human brain. *Sci Transl Med*. 2016;8:348ra96.

22. Carson R, Naganawa M, Matuskey D, et al. Age and sex effects on synaptic density in healthy humans as assessed with SV2A PET. *J Nucl Med*. 2018;59:541-541.

23. Chen M-K, Mecca AP, Naganawa M, et al. Assessing Synaptic Density in Alzheimer Disease With Synaptic Vesicle Glycoprotein 2A Positron Emission Tomographic Imaging. *JAMA Neurol*. 2018;75:1215-1224.

24. Kawamural K, Ishiwata K, Tajima H, et al. In vivo evaluation of [11C]SA4503 as a PET ligand for mapping CNS sigma1receptors. *Nucl Med Biol*. 2000;27:255-61.

25. Finnema SJ, Nabulsi, Mercier J, et al. Synthesis and Preclinical Evaluation of 11C-UCB-J as a PET Tracer for Imaging the Synaptic Vesicle Glycoprotein 2A in the Brain. *J Nucl Med*. 2016;57:777-784.

26. Jenkinson M, Pechaud M, Smith S. BET2: MR-based estimation of brain, skull and scalp surfaces. *Elev Annu Meet Organ Hum brain Mapp*. 2005.

27. Grabner G, Janke AL, Budge MM, Smith D, Pruessner J, Collins DL. Symmetric atlasing and model based segmentation: an application to the hippocampus in older adults. *Med Image Comput Comput Assist Interv*. 2006;9:58-66.

28. Tziortzi AC, Searle GE, Tzimopoulou S, et al. Imaging dopamine receptors in humans with [11C]-(+)-PHNO: Dissection of D3 signal and anatomy. *Neuroimage*. 2011; 54:264-77.

29. Tzourio-Mazoyer N, Landeau B, Papathanassiou D, et al. Automated anatomical labeling of activations in SPM using a macroscopic anatomical parcellation of the MNI MRI single-subject brain. *Neuroimage*. 2002;15:273-89.

30. Ichise M, Toyama H, Innis RB, Carson RE. Strategies to improve neuroreceptor parameter estimation by linear regression analysis. *J Cereb Blood Flow Metab*. 2002; 22:1271-81.

31. Akaike H. Information Theory and an Extension of the Maximum Likelihood Principle. *Int Symp Inf theory*. 1973:267-281.

32. Koole M, van Aalst J, Devrome M, et al. Quantifying SV2A density and drug occupancy in the human brain using [11C]UCB-J PET imaging and subcortical white matter as reference tissue. *Eur J Nucl Med Mol Imaging*. 2018; 46:396-406.

33. Finnema SJ, Nabulsi NB, Mercier J, et al. Kinetic evaluation and test–retest reproducibility of [^{11} C]UCB-J, a novel radioligand for positron emission tomography imaging of synaptic vesicle glycoprotein 2A in humans. *J Cereb Blood Flow Metab*. 2018;38:2041-2052.

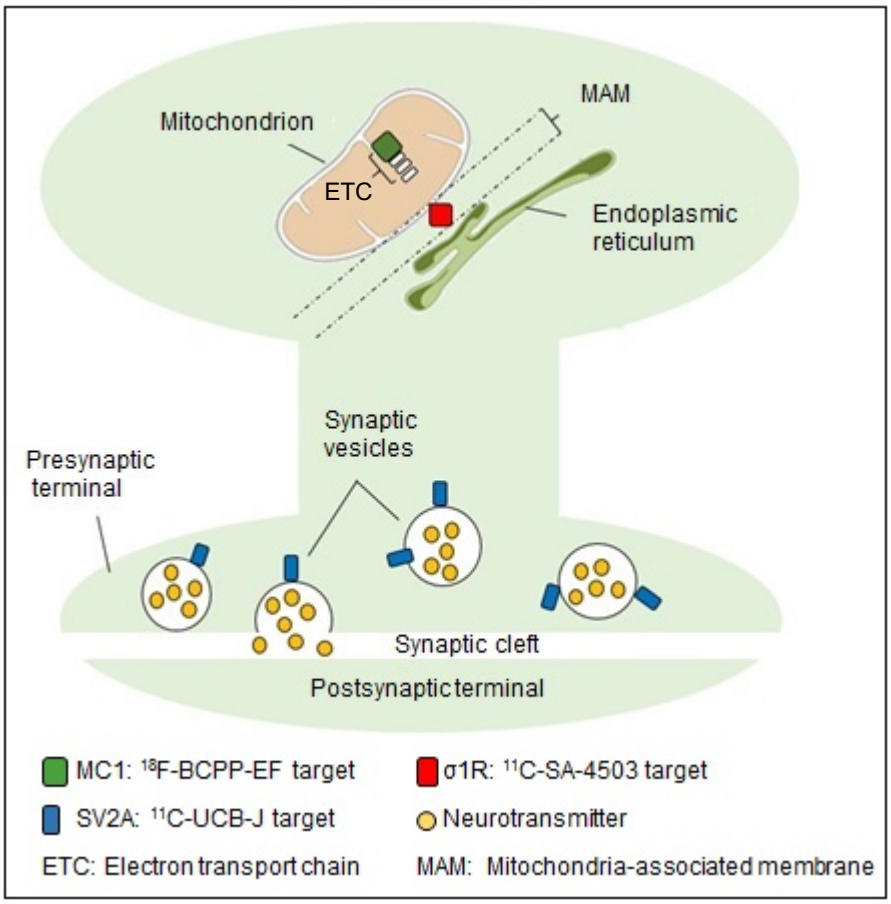

FIGURE 1. Mitochondrial-ER-Synaptic Axis.

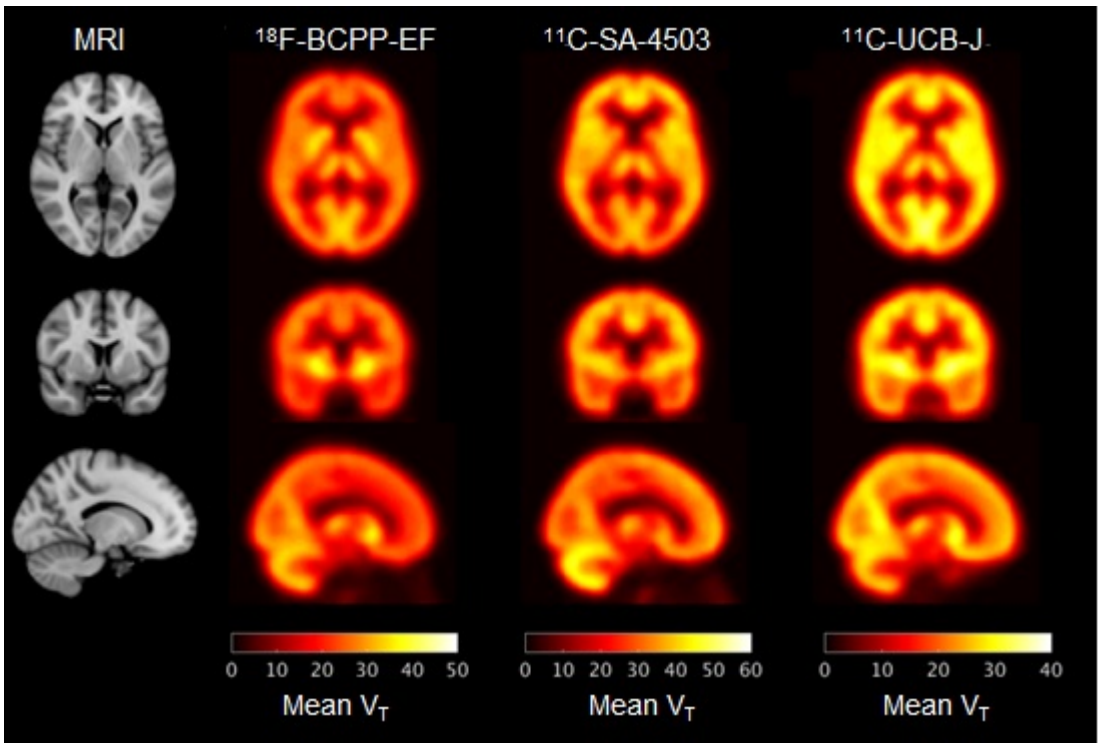

FIGURE 2. Orthogonal cross-sections of average parametric V_T images generated by 1TC (^{18}F-BCPP-EF) and Logan graphical Analysis (^{11}C-SA-4503,^{11}C-UCB-J).

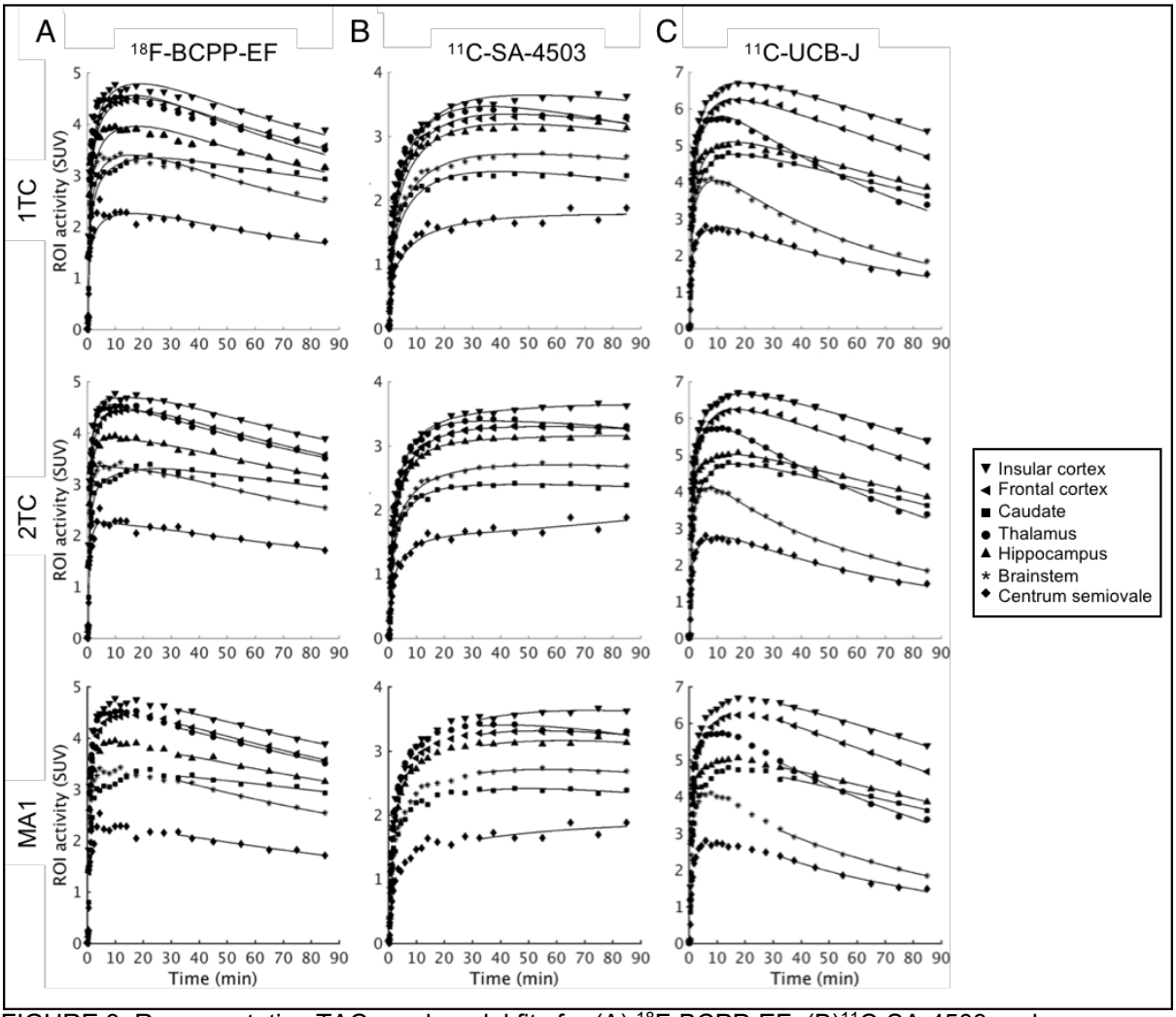

FIGURE 3. Representative TACs and model fits for (A) ^{18}F-BCPP-EF, (B)^{11}C-SA-4503 and (C)^{11}C-UCB-J

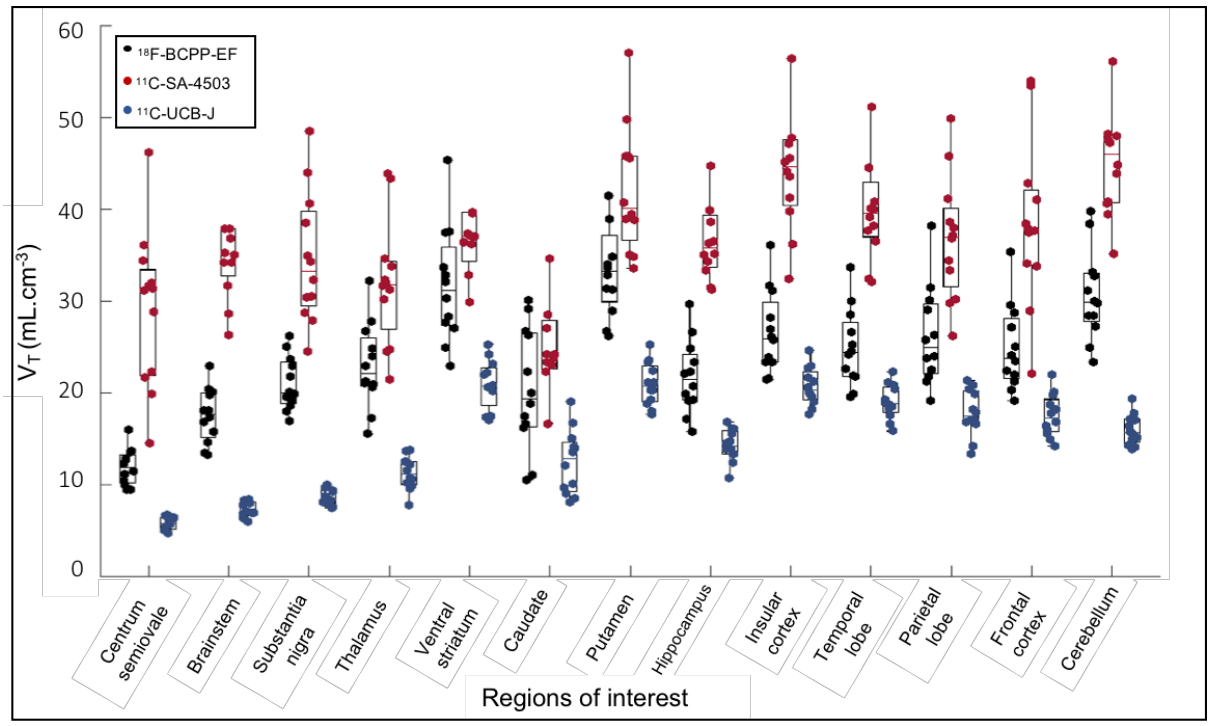

FIGURE 4. Distribution of individual regional V_T estimates for each radioligand.

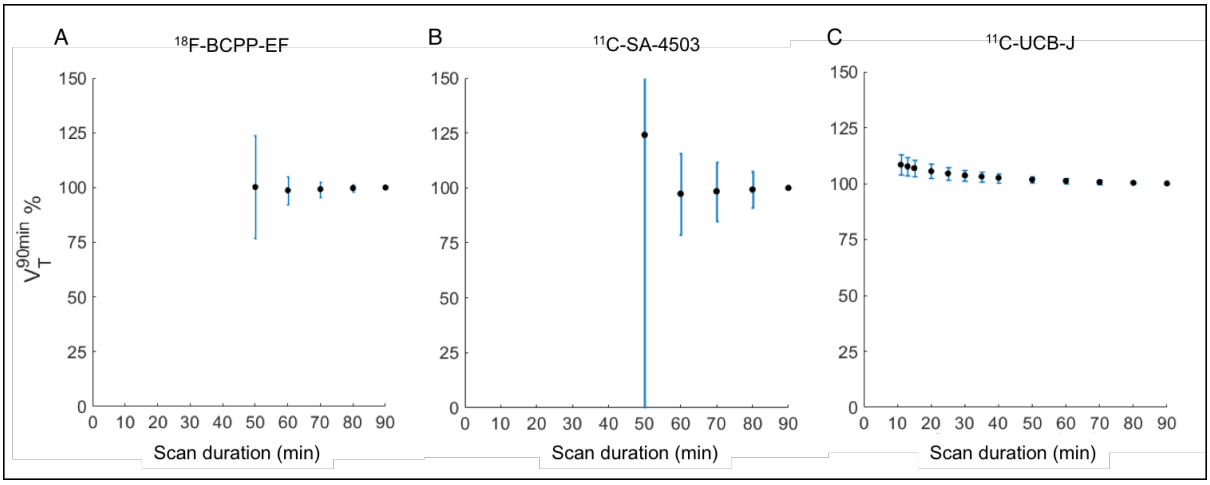

FIGURE 5. Time stability plots for (A)^{18}F-BCPP-EF, (B)^{11}C-SA-4503, and (C)^{11}C-UCB-J V_T estimates. n=156 data points. The first 50 minutes for ^{18}F-BCPP-EF and ^{11}C-SA-4503 have been excluded from the plots for clarity.

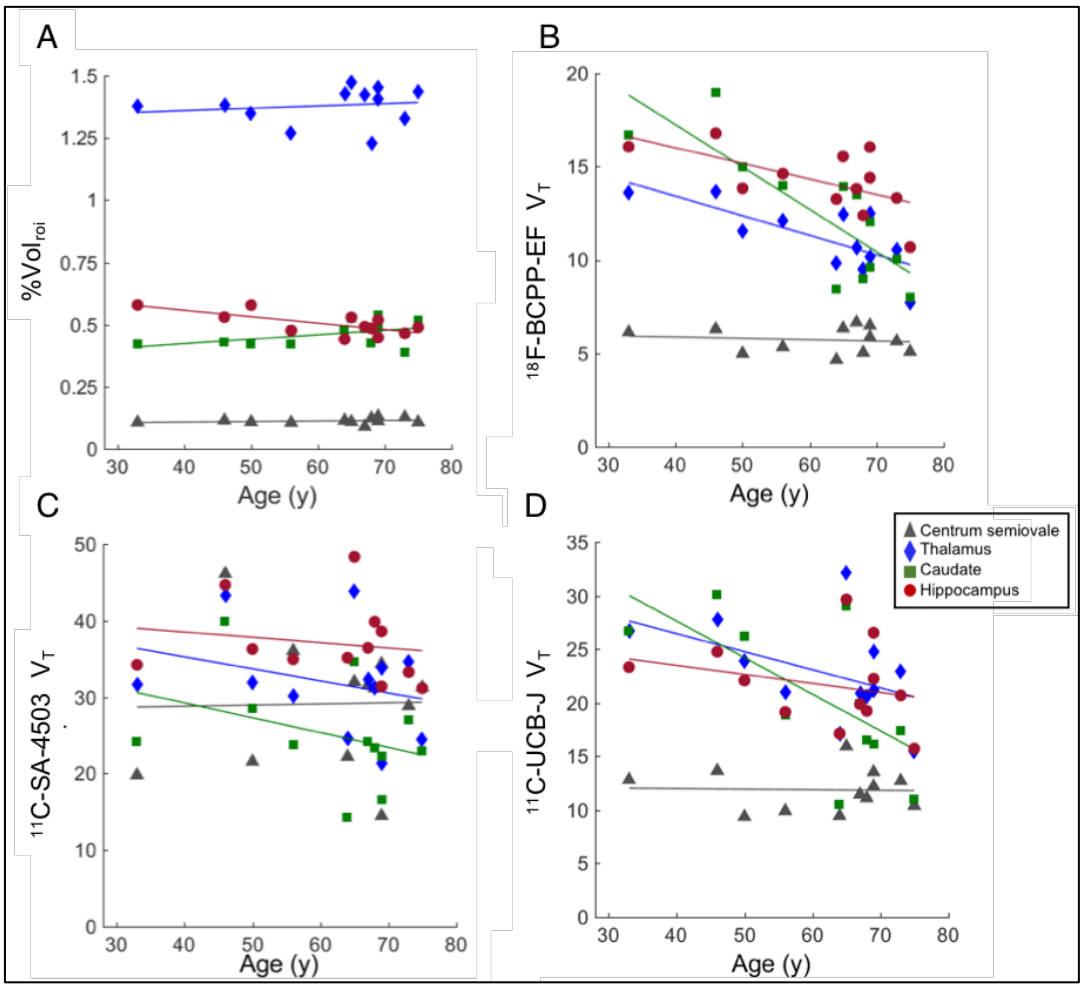

FIGURE 6. Linear regression plots of age vs (A) %Vol$_{roi}$, (B) ^{18}F-BCPP-EF V_T, (C) ^{11}C-SA-4503 V_T and (D)^{11}C-UCB-J V_T.

TABLE 1
V_T and $\%Vol_{roi}$ estimates

Radioligand	Kinetic model	Regions of interest												
		Centrum semiovale	Brain-stem	Substantia nigra	Thalamus	Ventral striatum	Caudate	Putamen	Hippocam-pus	Insular cortex	Temporal lobe	Parietal lobe	Frontal cortex	Cerebel-lum
^{18}F-BCPP-EF	1TC	10.8	16.2	19.2	21	29.6	19.2	31.9	19.6	24.9	23.1	24.5	23.3	28.5
		19%	17%	14%	21%	21%	32%	20%	19%	18%	18%	21%	19%	17%
	2TC	11.9	17.5	20.9	22.8	31.6	20.4	34.1	21.6	26.5	24.7	26	24.7	30.6
		17%	17%	14%	20%	20%	32%	18%	18%	17%	17%	20%	18%	16%
	MA1	11.9	17.5	20.9	22.9	31.6	20.4	34	21.7	26.6	24.8	26.1	24.8	30.6
		17%	17%	14%	20%	20%	32%	19%	18%	17%	17%	20%	19%	16%
^{11}C-SA-5403	1TC	23.2	31.7	30.5	28.6	34	22	37.4	32.5	39.4	35.7	33	34.6	41.7
		23%	18%	17%	21%	21%	31%	18%	16%	15%	16%	18%	23%	17%
	2TC	26.5	37.9	34	32.7	36.8	29.4	43.8	37.9	45.9	41.5	37.7	39.4	47.7
		31%	22%	17%	22%	19%	26%	17%	15%	16%	16%	19%	23%	19%
	MA1	29.1	36.5	34.6	31.9	37.9	25.1	42.1	37	44.6	40.4	36.7	38.4	46.5
		29%	20%	21%	21%	21%	28%	16%	14%	16%	16%	18%	23%	18%
^{11}C-UCB-J	1TC	5.7	7.2	8.5	11.2	20.9	12.4	20.9	13.4	20.5	17.6	15.5	14	15.9
		12%	12%	10%	16%	13%	28%	11%	13%	10%	10%	14%	14%	10%
	2TC	5.9	7.4	8.9	11.4	21.2	12.6	21.1	14.6	20.9	19.3	18	17.7	16.5
		11%	11%	10%	15%	12%	28%	11%	12%	9%	9%	14%	13%	9%
	MA1	5.8	7.4	8.8	11.5	21.2	12.6	21.1	14.6	20.9	19.3	18	17.7	16.5
		12%	11%	9%	15%	12%	28%	10%	13%	9%	9%	13%	13%	9%
$\%Vol_{roi}$		0.11	2.33	0.07	1.38	0.15	0.46	0.62	0.50	0.83	8.00	6.28	5.39	6.49
		10%	5%	7%	5%	6%	11%	7%	9%	9%	6%	9%	9%	7%

Data are mean and COV.17 values for ^{11}C-SA-4503 2TC estimation and 3 values for ^{11}C-UCB-J 2TC estimation were determined as unidentifiable and excluded (based on V_T of SE% > 10).

TABLE 2
Age effects on volumetric and PET outcome measures

ROI	$\%Vol_{roi}$			^{18}F-BCPP-EF			^{11}C-SA-4503			^{11}C-UCB-J		
	r	p	Δ/year	r	p	Δ/year	r	p	Δ/year	r	p	Δ/year
Centrum semiovale	0.26	0.42	0.2	-0.03	0.92	-0.05	0.02	0.95	0.05	-0.13	0.68	-0.13
Brainstem	0.14	0.65	0.05	-0.16	0.63	-0.21	-0.22	0.49	-0.35	-0.44	0.15	-0.41
Substantia nigra	-0.33	0.29	-0.17	0.02	0.94	0.03	-0.38	0.23	-0.62	-0.36	0.25	-0.28
Thalamus	0.16	0.62	0.07	-0.46	0.13	-0.74	-0.29	0.36	-0.49	-0.74	0.01*	-0.93
Ventral striatum	-0.18	0.57	-0.09	-0.25	0.44	-0.39	-0.24	0.45	-0.4	-0.62	0.03*	-0.63
Caudate	0.46	0.14	0.39	-0.65	0.02*	-1.68	-0.35	0.26	-0.77	-0.82	0.001**	-1.83
Putamen	-0.51	0.09	-0.27	-0.14	0.67	-0.21	-0.02	0.94	-0.03	-0.44	0.16	-0.39
Hippocampus	-0.48	0.11	-0.33	-0.27	0.4	-0.39	-0.17	0.6	-0.19	-0.61	0.04*	-0.59
Insular cortex	-0.41	0.19	-0.28	-0.26	0.41	-0.35	-0.21	0.52	-0.26	-0.6	0.04*	-0.48
Temporal lobe	-0.71	0.01*	-0.51	-0.26	0.42	-0.35	-0.2	0.54	-0.25	-0.55	0.06	-0.44
Parietal lobe	-0.77	0.003**	-0.36	-0.32	0.31	-0.52	-0.17	0.61	-0.24	-0.61	0.03*	-0.69
Frontal cortex	-0.75	0.01*	-0.53	-0.35	0.27	-0.52	-0.23	0.47	-0.43	-0.65	0.02*	-0.69
Cerebellum	-0.45	0.14	-0.25	0.02	0.96	0.02	-0.23	0.47	-0.33	-0.13	0.68	-0.11

r : correlation coefficient. * p<0.05; **p<0.005.

SUPPLEMENTAL DATA

Arterial Input function Modelling

Whole blood activity was measured using a continuous automatic blood sampling system (Allogg AB, Marlefred, Sweden) acquired at a rate of 5 mL/min for the first 15 minutes of the scan. Discrete blood samples were taken at 10, 15, 20, 25, 30, 40, 50, 60, 70, 80 and 90 minutes after scan start and total radioactivity concentration was evaluated in both blood and plasma in a Perkin Elmer 1470 10-well gamma counter. Discrete blood samples were used to determine the fraction of plasma radioactivity constituted by unchanged parent radioligand (*ppf*) using high-performance liquid chromatography analysis. For each ligand, the plasma free fraction (f_p) was measured by ultrafiltration in triplicate using an arterial blood sample taken prior to tracer injection.

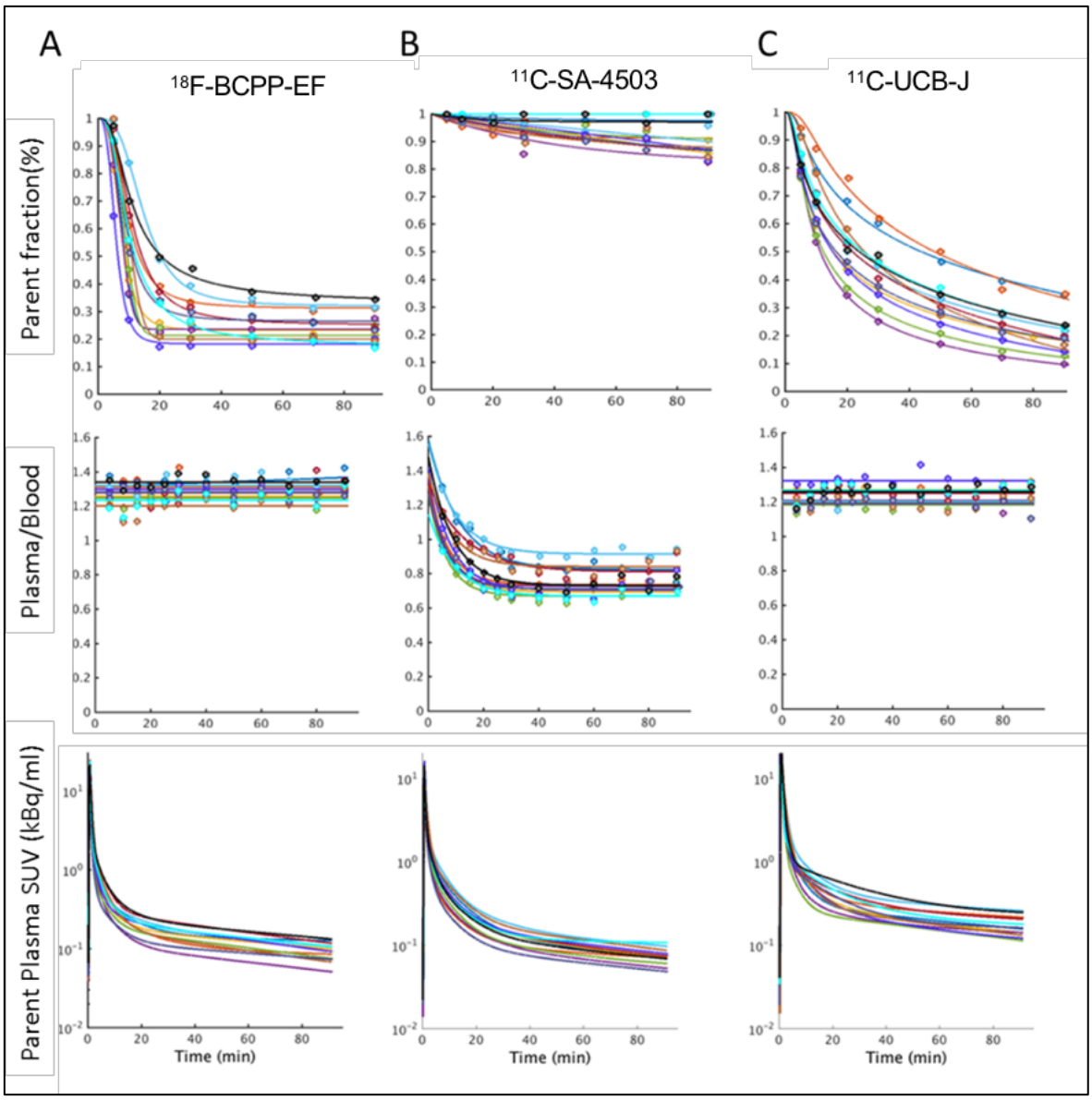

Supplemental Figure 1. Individual model fits to parent fraction, plasma/blood and input function data

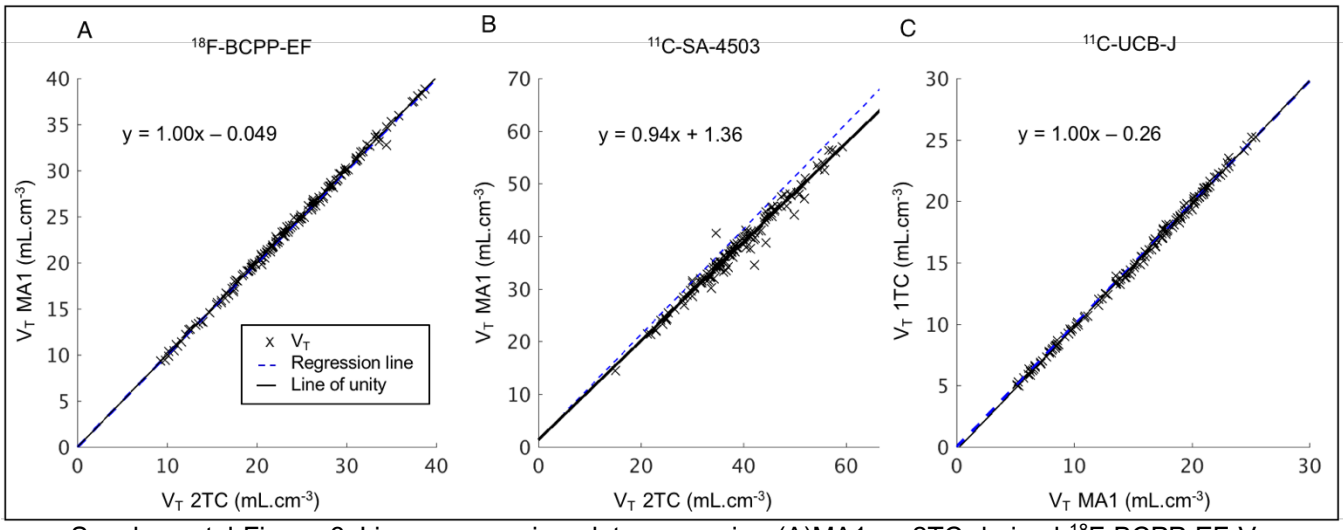

Supplemental Figure *2*. Linear regression plots comparing (A)MA1 vs 2TC derived ^{18}F-BCPP-EF V_T, (B)MA1 vs 2TC derived ^{11}C-SA-4503 V_T, (C)MA1 vs 1TC derived ^{11}C-UCB-J V_T.

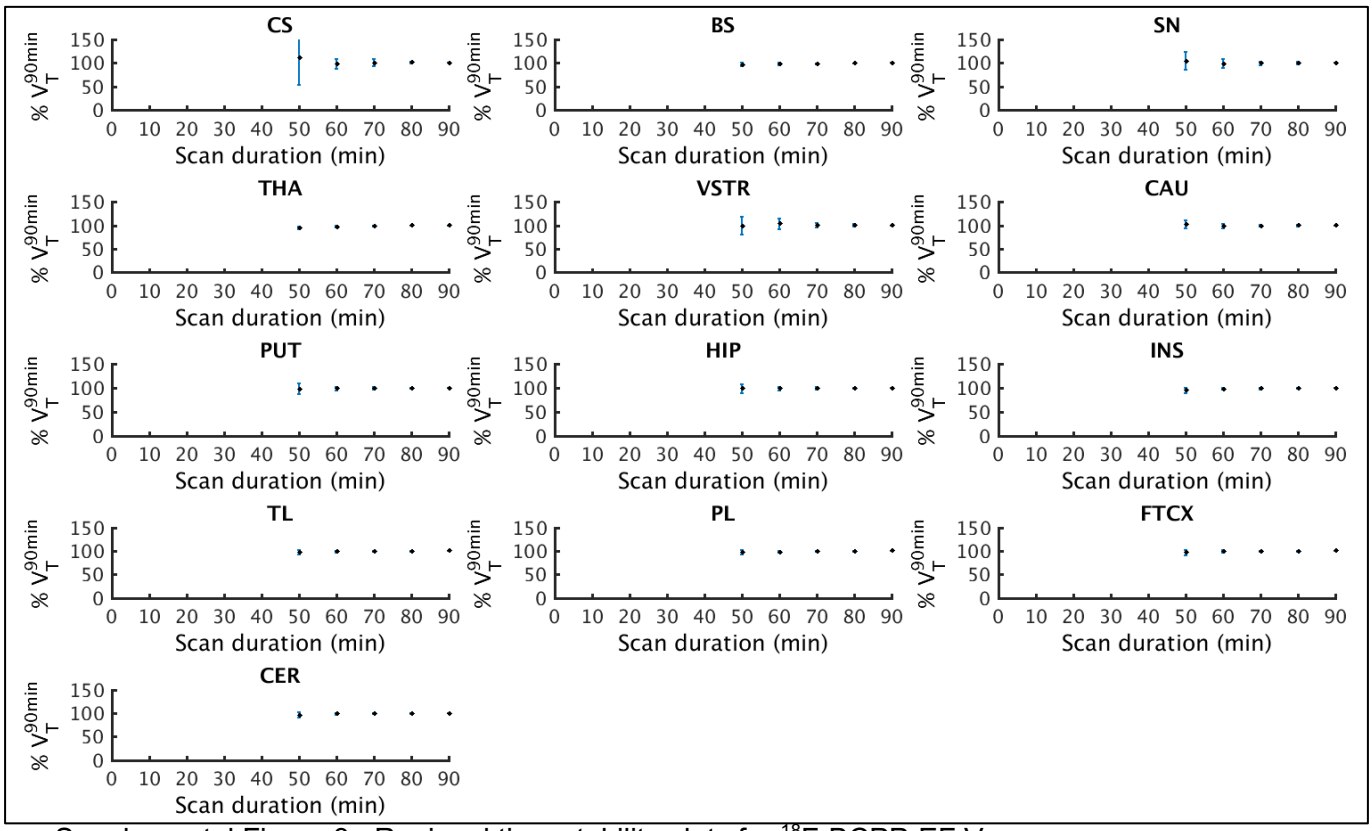

Supplemental Figure 3. Regional time stability plots for ^{18}F-BCPP-EF V_T.

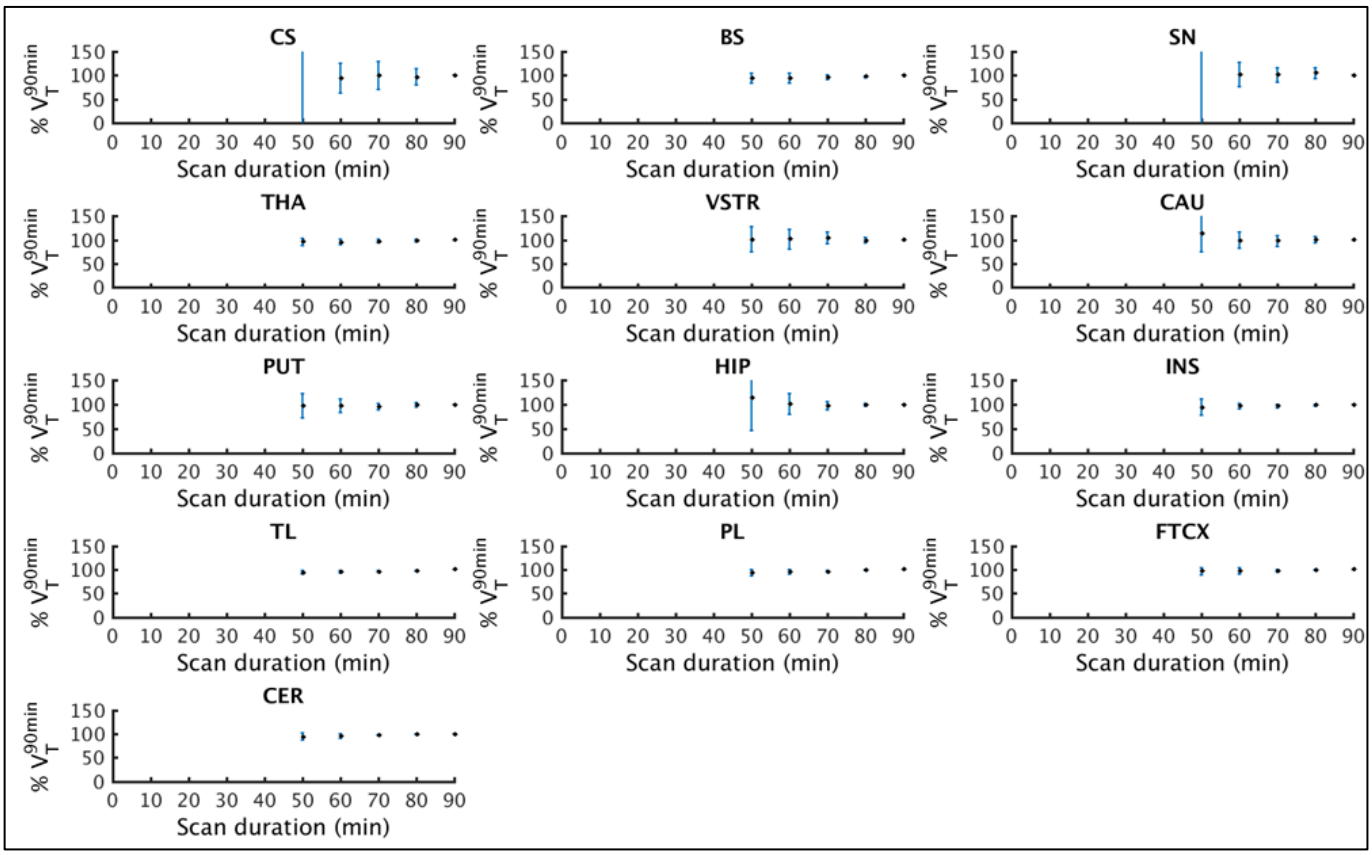

Supplemental Figure 4. Regional time stability plots for ^{11}C-SA-4503 V_T.

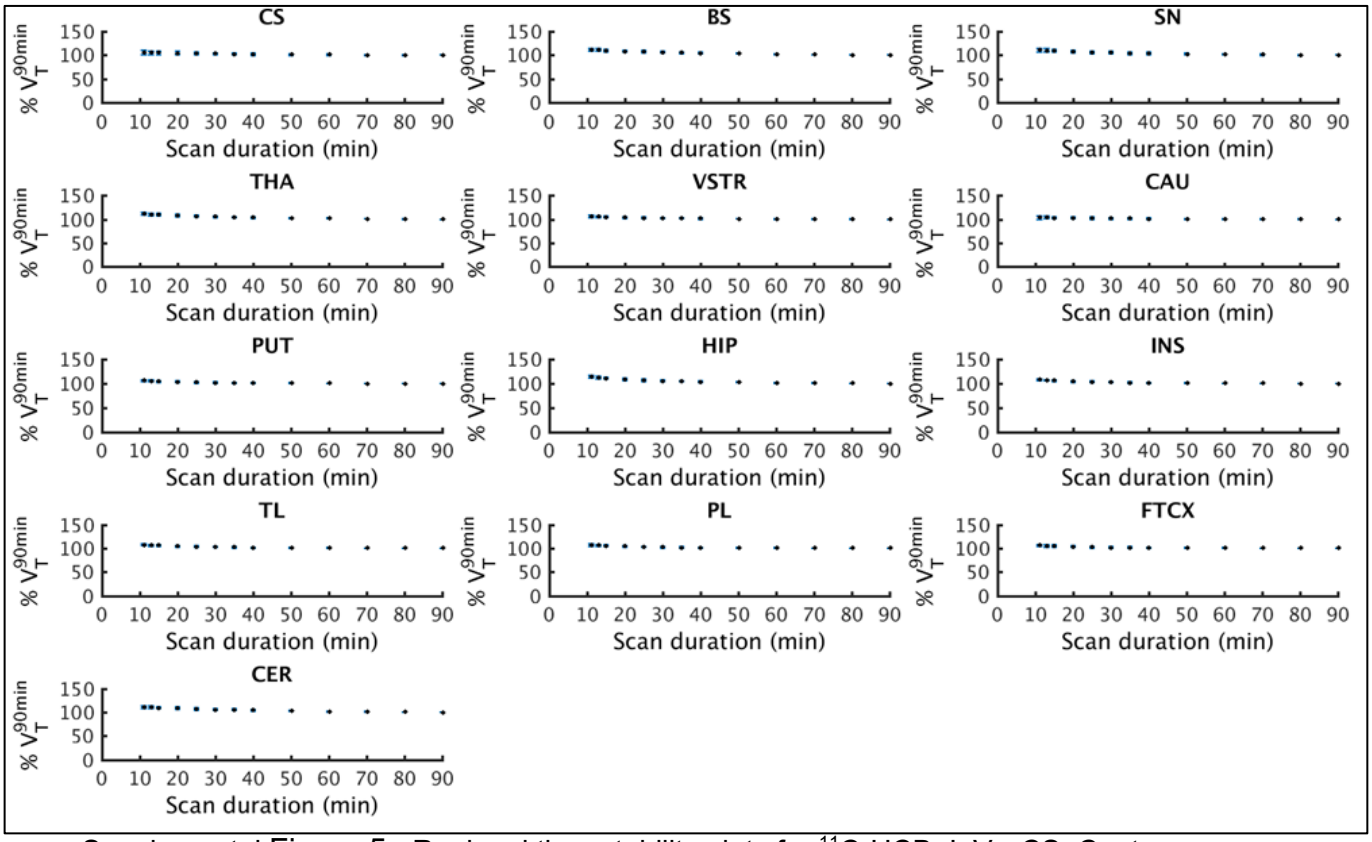

Supplemental Figure 5. Regional time stability plots for ^{11}C-UCB-J V_T. CS: Centrum semiovale, BST: Brainstem, SN: substantia nigra, THA: thalamus, VST: ventral striatum, CAU: caudate, PUT: putamen, HIP: hippocampus, INS: insular cortex, TI; temporal lobe, PL: parietal lobe, FTCX: frontal cortex, CER: cerebellum

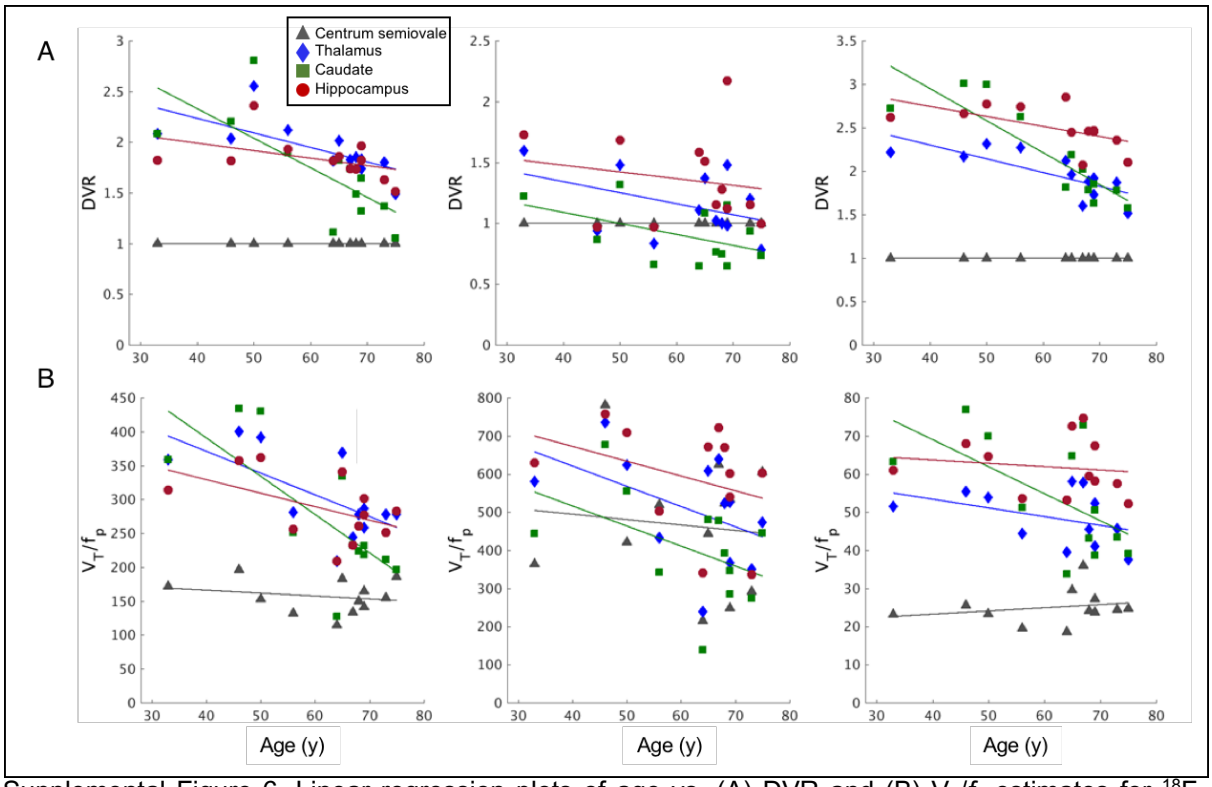

Supplemental Figure 6. Linear regression plots of age vs. (A) DVR and (B) V_T/f_p estimates for ^{18}F-BCPP-EF for ^{11}C-SA-4503 and for ^{11}C-UCB-J.

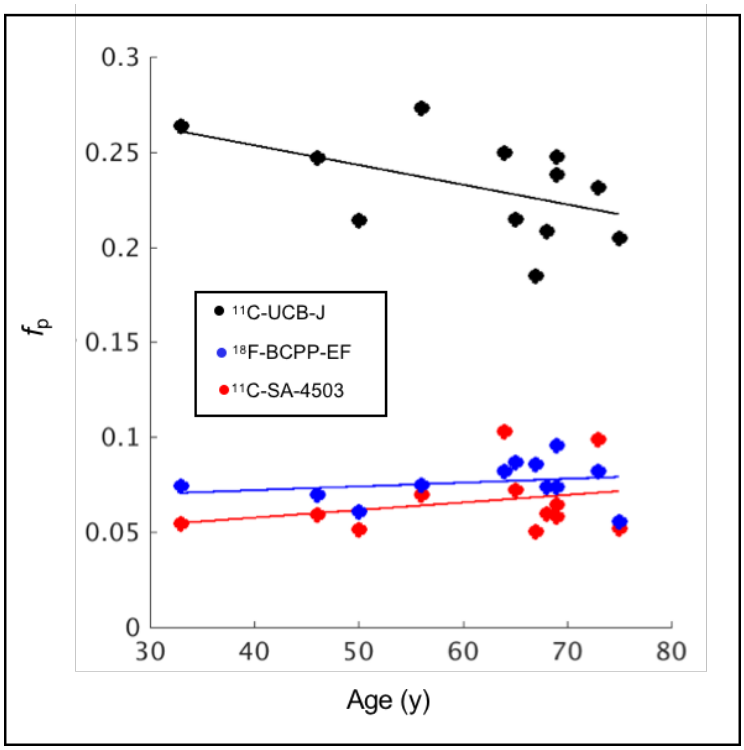

Supplemental Figure 7. Linear regression plots for age vs f_p

Supplemental Table 1. Demographic information and individual scan parameters

Demographic Data			Scan parameters								
			^{18}F-BCPP-EF			^{11}C-SA-4503			^{11}C-UCB-J		
Sex	Age (y)	MMSE score	Inj. Act (MBq)	Inj. Mass (μg)	f_p	Inj. Act (MBq)	Inj. Mass (μg)	f_p	Inj. Act (MBq)	Inj. Mass (μg)	f_p
M	56	29	87	0.03	0.07	257	3.10	0.07	250	3.43	0.27
M	75	30	94	0.04	0.06	281	2.82	0.05	234	1.85	0.21
F	67	29	89	0.04	0.09	267	2.29	0.05	176	1.61	0.19
F	65	30	97	0.13	0.09	277	5.23	0.07	113	1.45	0.21
M	46	29	91	0.07	0.07	244	2.41	0.06	191	2.05	0.25
M	69	28	87	0.06	0.07	221	2.86	0.06	261	6.26	0.25
M	68	28	91	0.05	0.07	229	1.84	0.06	234	1.82	0.21
F	50	30	91	0.05	0.06	255	2.01	0.05	230	2.12	0.21
F	69	30	96	0.11	0.10	236	1.47	0.06	278	2.23	0.24
F	33	30	85	0.04	0.07	219	5.43	0.05	249	2.60	0.26
M	73	29	82	0.09	0.08	252	3.28	0.10	245	3.53	0.23
M	64	28	88	0.12	0.08	277	3.10	0.10	152	2.54	0.25
Mean	61	29	90	0.07	0.08	251	2.99	0.07	218	2.62	0.23
SD	13	1	4	0.03	0.01	22	1.23	0.02	49	1.32	0.03
COV	20%	3%	5%	50%	16%	9%	41%	27%	23%	50%	11%

f_p = plasma free fraction; MMSE – Mini-Mental state exam
* Radiochemical purities were over 98% for all three tracers.

Supplemental Table 2. Mass effects on PET outcome measures

ROI	^{18}F-BCPP-EF		^{11}C-SA-4503		^{11}C-UCB-J	
	r	p	*r*	p	*r*	p
Centrum semiovale	0.50	0.10	-0.26	0.42	-0.07	0.83
Brainstem	0.42	0.17	0.33	0.29	0.10	0.75
Substantia nigra	0.69	0.01	0.32	0.32	0.19	0.55
Thalamus	0.36	0.25	0.21	0.51	-0.10	0.76
Ventral striatum	0.45	0.14	0.32	0.31	-0.09	0.78
Caudate	0.08	0.80	0.16	0.62	-0.25	0.44
Putamen	0.56	0.06	0.22	0.49	-0.11	0.74
Hippocampus	0.49	0.10	0.14	0.67	0.05	0.88
Insular cortex	0.52	0.09	0.05	0.87	0.01	0.98
Temporal lobe	0.51	0.09	0.14	0.66	0.01	0.97
Parietal lobe	0.52	0.08	0.19	0.56	0.07	0.83
Frontal cortex	0.47	0.12	0.18	0.57	0.00	0.99
Cerebellum	0.50	0.10	0.37	0.24	0.16	0.61

r = correlation coefficient

Supplemental Table 3. DVR estimates from 1TC, 2TC and MA1

Radioligand	Kinetic model	Regions of interest											
		BST	SN	THA	VST	CAU	PUT	HIP	INS	TL	PL	FTCX	CER
^{18}F-BCPP-EF	1TC	1.51	1.79	1.95	2.73	1.77	2.96	1.82	2.31	2.15	2.27	2.17	2.65
		10%	9%	12%	10%	27%	9%	11%	9%	10%	10%	9%	8%
	2TC	1.47	1.76	1.92	2.65	1.71	2.86	1.82	2.23	2.08	2.17	2.07	2.58
		12%	8%	13%	11%	28%	9%	11%	9%	10%	9%	8%	10%
	MA1	1.58	1.78	1.93	2.67	1.71	2.87	1.83	2.25	2.10	2.19	2.09	2.59
		12%	10%	14%	12%	29%	10%	11%	10%	10%	10%	9%	10%
^{11}C-SA-5403	1TC	1.43	1.39	1.26	1.50	0.96	1.66	1.45	1.76	1.60	1.47	1.53	1.88
		18%	21%	14%	14%	24%	14%	17%	15%	16%	15%	14%	19%
	2TC	1.59	1.44	1.27	1.49	1.04	1.81	1.58	1.87	1.71	1.51	1.52	2.04
		25%	38%	18%	16%	28%	18%	25%	17%	21%	19%	14%	24%
	MA1	1.34	1.28	1.15	1.36	0.90	1.54	1.36	1.62	1.47	1.33	1.37	1.71
		31%	35%	24%	23%	27%	26%	28%	22%	26%	25%	22%	31%
^{11}C-UCB-J	1TC	1.26	1.50	1.96	3.66	2.17	3.67	2.50	3.63	3.34	3.11	3.07	2.80
		7%	8%	13%	8%	24%	7%	10%	9%	8%	11%	10%	8%
	2TC	1.27	1.49	1.92	3.58	2.09	3.54	2.44	3.51	3.24	3.00	2.95	2.81
		6%	8%	14%	7%	23%	6%	9%	8%	8%	10%	9%	7%
	MA1	1.28	1.52	1.98	3.63	2.15	3.62	2.53	3.61	3.32	3.08	3.03	2.84
		7%	8%	13%	7%	24%	7%	10%	8%	8%	10%	10%	8%

*17 values for ^{11}C-SA-4503 2TC estimation and 3 values for ^{11}C-UCB-J 2TC estimation were determined as unidentifiable and excluded (based on V_T of SE% > 10).

BST: Brainstem, SN: substantia nigra, THA: thalamus, VST: ventral striatum, CAU: caudate, PUT: putamen, HIP: hippocampus, INS: insular cortex, TI; temporal lobe, PL: parietal lobe, FTCX: frontal cortex, CER: cerebellum

Supplemental Table 4. V_T/f_p estimates from 1TC, 2TC and MA1

Radioligand	Kinetic model	Regions of interest												
		CS	BST	SN	THA	VST	CAU	PUT	HIP	INS	TL	PL	FTCX	CER
^{18}F-BCPP-EF	1TC	143	214	254	278	391	255	422	259	329	306	323	309	377
		16%	17%	14%	21%	20%	35%	18%	18%	17%	17%	18%	18%	15%
	2TC	157	232	277	302	418	271	451	286	351	328	343	327	405
		15%	18%	14%	20%	19%	35%	17%	17%	17%	17%	17%	18%	15%
	MA1	157	232	277	303	419	271	450	287	352	329	344	329	405
		16%	18%	14%	20%	20%	35%	17%	17%	17%	17%	18%	18%	15%
^{11}C-SA-5403	1TC	372	509	488	455	543	354	596	518	630	572	526	553	668
		30%	27%	26%	27%	27%	37%	25%	24%	26%	26%	26%	29%	27%
	2TC	456	611	544	520	605	476	698	608	736	664	598	628	765
		28%	30%	20%	27%	30%	27%	25%	24%	27%	26%	25%	29%	27%
	MA1	465	588	553	508	604	405	671	590	714	647	584	614	747
		36%	29%	29%	28%	27%	35%	25%	23%	26%	26%	26%	30%	27%
^{11}C-UCB-J	1TC	25	31	37	49	91	54	91	62	90	83	77	76	69
		18%	13%	12%	15%	15%	28%	14%	12%	12%	11%	13%	13%	12%
	2TC	26	32	39	50	92	55	92	63	91	84	78	77	72
		17%	13%	11%	14%	15%	27%	13%	12%	10%	11%	13%	13%	12%
	MA1	25	32	38	50	92	54	91	64	91	84	78	76	72
		17%	13%	11%	15%	15%	27%	13%	12%	10%	11%	13%	13%	12%

*17 values for ^{11}C-SA-4503 2TC estimation and 3 values for ^{11}C-UCB-J 2TC estimation were determined as unidentifiable and excluded (based on V_T of SE% > 10).

CS: centrum semiovale, BST: brainstem, SN: substantia nigra, THA: thalamus, VST: ventral striatum, CAU: caudate, PUT: putamen, HIP: hippocampus, INS: insular cortex, TI; temporal lobe, PL: parietal lobe, FTCX: frontal cortex, CER: cerebellum

Supplemental Table 5. Age effect on DVR

ROI	^{18}F-BCPP-EF			^{11}C-SA-4503			^{11}C-UCB-J		
	r	p	Δ/year	*r*	p	Δ/year	*r*	p	Δ/year
Brainstem	-0.25	0.43	-0.23	-0.25	0.43	-0.62	-0.5	0.1	-0.28
Substantia nigra	0.03	0.92	0.03	-0.31	0.33	-0.87	-0.24	0.46	-0.15
Thalamus	-0.69	0.01*	-0.74	-0.42	0.18	-0.79	-0.76	0.004**	-0.81
Ventral striatum	0.44	0.16	-0.4	-0.39	0.21	-0.7	-0.81	0.001**	-0.50
Caudate	-0.73	0.01*	-1.7	-0.47	0.12	-1.01	-0.87	0.0002**	-1.70
Putamen	-0.29	0.35	-0.23	-0.13	0.69	-0.27	-0.46	0.13	-0.26
Hippocampus	-0.45	0.14	-0.41	-0.18	0.57	-0.4	-0.59	0.04*	-0.46
Insular cortex	-0.44	0.15	-0.35	-0.3	0.35	-0.53	-0.5	0.1	-0.34
Temporal lobe	-0.44	0.15	-0.36	-0.24	0.44	-0.5	-0.47	0.13	-0.31
Parietal lobe	-0.64	0.02*	-0.51	-0.28	0.39	-0.54	-0.65	0.02*	-0.56
Frontal cortex	-0.71	0.01*	-0.49	-0.44	0.15	-0.77	-0.68	0.02*	-0.54
Cerebellum	-0.004	0.99	-0.003	-0.25	0.43	-0.63	0.01	0.98	0.01

DVR results for ^{18}F-BCPP-EF, ^{11}C-SA-4503 and ^{11}C-UCB-J calculated from MA1, MA1 and 1TC-derived V_T estimates.
r = correlation coefficient, *p<0.05, **p<0.005

Supplemental Table 6. Age effect on V_T/f_p

ROI	^{18}F-BCPP-EF			^{11}C-SA-4503			^{11}C-UCB-J		
	r	p	Δ/year	*r*	p	Δ/year	*r*	p	Δ/year
Centrum semiovale	-0.22	0.49	-0.27	-0.11	0.74	-0.31	0.23	0.47	0.33
Brainstem	-0.35	0.27	-0.5	-0.35	0.26	-0.83	0.04	0.9	0.05
Substantia nigra	-0.22	0.5	-0.24	-0.51	0.09	-1.18	0.17	0.59	0.16
Thalamus	-0.66	0.02*	-1.06	-0.47	0.12	-1.05	-0.4	0.2	-0.47
Ventral striatum	-0.44	0.15	-0.69	-0.42	0.17	-0.9	-0.14	0.67	-0.17
Caudate	-0.74	0.01*	-2.09	-0.47	0.13	-1.3	-0.6	0.04*	-1.31
Putamen	-0.37	0.24	-0.5	-0.26	0.41	-0.52	0.06	0.86	0.06
Hippocampus	-0.51	0.09	-0.7	-0.35	0.26	-0.66	-0.15	0.65	-0.14
Insular cortex	-0.45	0.14	-0.63	-0.35	0.27	-0.73	-0.03	0.93	-0.03
Temporal lobe	-0.47	0.12	-0.64	-0.35	0.26	-0.73	0.01	0.98	0.01
Parietal lobe	-0.57	0.05*	-0.81	-0.38	0.22	-0.78	-0.23	0.47	-0.24
Frontal cortex	-0.54	0.07	-0.79	-0.4	0.2	-0.96	-0.22	0.5	-0.22
Cerebellum	-0.21	0.52	-0.25	-0.38	0.23	-0.82	0.32	0.31	0.31

V_T/f_p results for ^{18}F-BCPP-EF, ^{11}C-SA-4503 and ^{11}C-UCB-J calculated from MA1, MA1 and 1TC-derived V_T estimates.
r = correlation coefficient, *p<0.05, **p<0.005

Supplemental Table 7. Age effects on V_T with regional volume as covariate

ROI	^{18}F-BCPP-EF		^{11}C-SA-4503		^{11}C-UCB-J	
	r	p	*r*	p	*r*	p
Centrum semiovale	-0.10	0.77	-0.01	0.99	-0.10	0.77
Brainstem	-0.24	0.48	-0.22	0.52	-0.56	0.08
Substantia nigra	0.17	0.62	-0.37	0.27	-0.18	0.61
Thalamus	-0.50	0.11	-0.31	0.36	-0.76	0.01*
Ventral striatum	-0.18	0.59	-0.20	0.55	-0.61	0.05*
Caudate	-0.63	0.04*	-0.26	0.44	-0.78	0.004**
Putamen	-0.02	0.94	0.03	0.94	-0.34	0.31
Hippocampus	-0.11	0.74	0.02	0.95	-0.49	0.13
Insular cortex	-0.13	0.71	-0.20	0.56	-0.60	0.05
Temporal lobe	0.23	0.51	0.23	0.50	-0.36	0.28
Parietal lobe	-0.27	0.43	0.25	0.45	-0.66	0.03*
Frontal cortex	0.13	0.71	0.16	0.64	-0.40	0.22
Cerebellum	0.22	0.51	-0.05	0.89	-0.06	0.85

r = correlation coefficient
*P<0.05, **p<0.005